three standard reflections measured every 60 min; drift corrections (from standards), 1.092–1.006. No absorption corrections were applied (μ = 0.194 mm^{-1}) because Ψ scans suggested that the absorption was not severe.

All atoms including H atoms were located from Patterson and electron-density synthesis.[24] In the final cycles of least-squares refinement, 391 parameters were refined, including positional and anisotropic thermal parameters[25] for all non-hydrogen atoms. The hydrogen atoms were placed at positions that gave the closest agreement with the peaks found in difference Fourier maps (C–H = 0.97 Å, B–H = 0.97 Å), except for H9, which was positioned at the location found from a difference map. In the last cycle of refinement, one parameter [H2N, x coordinate] shifted by 1.6 σ, and another [H2N, y coordinate] shifted by 1.1 σ; the largest shift of all other atoms was 0.07 σ. Convergence was achieved with R = 0.077 and R_w = 0.070.[26] The highest peak on the final difference electron-density map (0.19 e Å^{-3}) was located between C54 and C55 of a piperidino side group. Complex scattering factors, corrected for anomalous dispersion, were used.[27]

Acknowledgment. This work was supported by a grant from NASA Ames Research Center.

Registry No. 1 (X = Cl; R = Me), 74721-85-0; **1** (X = Cl; R = Ph), 74721-87-2; **3** (R = Me), 84393-75-9; **3** (R = Ph), 84393-77-1; **4**, 940-71-6; **5**, 68351-74-6; **6**, 77217-45-9; **7**, 84254-25-1; **8**, 84393-78-2; **9**, 84393-79-3; **10**, 84416-56-8; **11**, 84369-00-6; **12** (M = Mo), 84416-58-0; **12** (M = W), 84416-60-4; **13** polymer, 84254-26-2; **13** repeating unit, 84254-27-3; **14**, 84332-49-0; **15**, 84393-80-6; **17** (M = Mo), 84393-82-8; **17** (M = W), 84393-84-0; $Rh(PPh_3)_3Cl$, 14694-95-2; $[n\text{-}Bu_3PCuI]_4$, 59245-99-7; $Rh(H)(PPh_3)_3$, 16973-49-2; $W(CO)_6$, 14040-11-0; $Mo(CO)_6$, 13939-06-5; NaH, 7646-69-7; 1-hexene, 592-41-6; n-hexane, 110-54-3; piperidine, 110-89-4; methylmagnesium chloride, 676-58-4; methylmagnesium bromide, 75-16-1; propargyl bromide, 106-96-7; decaborane, 17702-41-9; triethylamine, 121-44-8.

Supplementary Material Available: Tables of observed and calculated structure factors, positional and thermal parameters, and bond length and angles for **8** (22 pages). Ordering information is given on any current masthead page.

(24) All programs used in data collection reduction and refinement are part of the Enraf-Nonius Structure Determination Package, Enraf-Nonius, Delft, The Netherlands, 1975 (revised 1977).

(25) Anisotropic thermal parameters are of the form $\exp(-2\pi^2(U_{11}h^2(a^*)^2 + \ldots + 2U_{23}klb^*c^*))$. Isotropic thermal parameters are of the form $\exp(-B(\sin^2\theta)/\pi^2)$.

(26) $R = \sum(||F_o| - |F_c||)/\sum|F_o|$; $R_w = [\sum w(|F_o| - |F_c|)^2/\sum w(F_o)^2]^{1/2}$; $\sum w = 1/\sigma(F_o)^2$.

(27) "International Tables for X-ray Crystallography", 3rd ed.; Kynoch Press: Birmingham, England, 1968; Vol. III.

Iron- and Ruthenium-Linked Phosphazenes[1]

Harry R. Allcock,* Linda J. Wagner, and Michael L. Levin

Contribution from the Department of Chemistry, The Pennsylvania State University, University Park, Pennsylvania 16802. *Received June 14, 1982*

Abstract: A series of new organometallic phosphazenes that contains Fe–P, Ru–P, Ru–Ru, and Fe–Ru bonds has been isolated. The anions $[Fe(CO)_2Cp]^-$ and $[Ru(CO)_2Cp]^-$ react with $(NPF_2)_3$ (**2**) to replace first one and then two (geminal) fluorine atoms by $M(CO)_2Cp$ groups. The monoruthenium derivative (**5**) reacts with $[Fe(CO)_2Cp]^-$ to form a geminal, mixed-metal organometallic phosphazene (**7**) that, on photolysis, undergoes decarbonylation to an Fe–Ru bonded derivative (**8**). The monoiron cyclotriphosphazene (**9**) does not yield the same mixed-metal species when treated with $[Ru(CO)_2Cp]^-$ but instead forms the new mixed-metal dimer, $FeRu(CO)_4Cp_2$ (**10**). This dimer can also be prepared by the reaction of $[Ru(CO)_2Cp]^-$ with $Fe(CO)_2CpI$. Species **8** and its diiron analogue, **4**, undergo metal–metal bond cleavage with carbon monoxide. Species **7** and **8** are the first examples of phosphazenes with two different metals linked to a phosphazene ring. The new compounds were characterized by ^{31}P, ^{19}F, and ^1H NMR, infrared, and mass spectral techniques. In addition, an X-ray crystal structure analysis of the mixed-metal phosphazene **8** was carried out. The Fe–Ru bond distance in **8** is 2.698 (1) Å and the Fe–P–Ru bond angle is 73.93 (2)°. Evidence was obtained that the organometallic unit perturbs the structure of the phosphazene ring.

Our long-range objective is the synthesis of inorganic high polymers of type **1**, in which transition-metal organometallic units

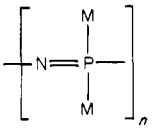

1

(M) form the side groups covalently attached to a long phosphazene chain. If such macromolecules could be synthesized, they would be of considerable interest as prospective polymeric catalysts or electroactive materials.

The synthesis of high polymers of type **1** is a complex undertaking. Until recently[2–4] no reactions were known that would link transition metals to phosphazenes through a P–M covalent bond. Moreover, the realities of polymer synthesis require that species such as **1** must be prepared either by the ring-opening polymerization of cyclic oligomeric analogues[5] or by substitution reactions carried out on a preformed macromolecular chain.[6] In either case, the first step is the development of procedures at the small-molecule level that would permit a wide range of metals to be linked to a phosphazene ring. If the polymer substitution route to **1** is later preferred, these small-molecule reactions will function as models for the macromolecular interactions.[7]

Recently we reported the synthesis and molecular structure determination of two small-molecule phosphazenes (**3** and **4**) that contain phosphorus–iron bonds.[2,3] These are prototypes for a wide range of similar derivatives that contain other transition metals.

(1) This work was presented, in part, at the 182nd National Meeting of the American Chemical Society, New York, Aug 23–28, 1981. This paper is part of a series on phosphorus–nitrogen ring systems and high polymers.

(2) Allcock, H. R.; Greigger, P. P. *J. Am. Chem. Soc.* **1979**, *101*, 2492.

(3) Allcock, H. R.; Greigger, P. P.; Wagner, L. J.; Bernheim, M. Y. *Inorg. Chem.* **1981**, *20*, 716.

(4) Schmidpeter, A.; Blanck, K.; Hess, H.; Riffel, H. *Angew. Chem.* **1980**, *92*, 655.

(5) Allcock, H. R. *Polymer* **1980**, *21*, 673.

(6) Allcock, H. R. *Angew. Chem., Int. Ed. Eng.* **1977**, *16*, 147.

(7) Allcock, H. R. *Acc. Chem. Res.* **1979**, *12*, 351.

0002-7863/83/1505-1321$01.50/0

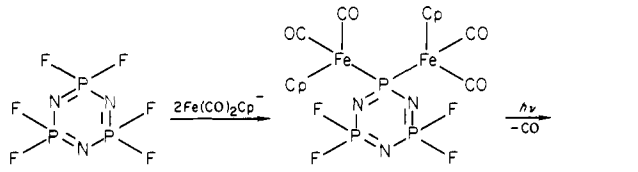

2 3

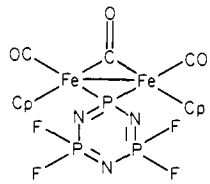

4

In this paper we extend this principle to ruthenium analogues and to the formation of analogues of **3** and **4** that contain two different metals.

Specifically, it was hoped to answer the following questions: (a) Are the reactions that lead to **3** or **4** unique, or can other metals be attached to the phosphazene skeleton? (b) If so, what problems associated with changes in metal size or organometallic nucleophilicity might be encountered? (c) What structural influence, if any, does the organometallic unit exert on the phosphazene ring, and vice versa? (d) Can **4** or its analogues that contain other metals be converted to species of type **3** when treated with carbon monoxide? The catalytic implications of this question are obvious. And (e), what pathways exist for the decomposition of species of type **3** or **4** either during their formation or at high temperatures? This question has a bearing on the synthesis of the high polymeric analogues.

Results and Discussion

The Synthetic Pathway. The cyclotriphosphazene **2** reacted with an equimolar amount of $[Ru(CO)_2Cp]^-$ with replacement of one fluorine atom by the organometallic unit to give the colorless product **5**, in approximately 15% yield (Scheme I). A considerable amount of the organometallic dimer, $Ru_2(CO)_4Cp_2$ was also isolated. The formation of this product will be discussed later.

Species **5** is a key reaction intermediate because it lies on the pathway to the formation of diruthenium phosphazenes on the one hand or mixed-metal derivatives on the other. Moreover, its reactivity and its resistance to skeletal cleavage during further reactions are of interest with respect to the eventual synthesis of polymers of type **1**.

Compound **5** appears to be less reactive than $(NPF_2)_3$ toward the $[Ru(CO)_2Cp]^-$ anion. However, **5** reacted with additional $[Ru(CO)_2Cp]^-$ anion with replacement of the geminal fluorine atom and the low-yield formation of the yellow, air-stable dimetallic Ru–Ru-bonded species **6**. Again the organometallic dimer, $Ru_2(CO)_4Cp_2$, was formed as a byproduct. Compound **6** is an analogue of the spirodiiron derivative **4** reported earlier. The nonspirodiruthenium species corresponding to **3** was not detected even when the reaction was conducted entirely in the dark. Possible reasons for this will be considered later. An alternative pathway to nonbridged (i.e., nonspiro) dimetallo derivatives is by the CO-induced metal–metal bond cleavage of species such as **4** or **6**, and this prospect is discussed later.

The formation of mixed-metal phosphazene derivatives was accomplished by the interaction of **5** with $[Fe(CO)_2Cp]^-$ (Scheme I). Again, the geminal fluorine atom was replaced to yield the yellow, air-stable species **7**. The organometallic dimer, $Fe_2(CO)_4Cp_2$, was also isolated from this reaction. Compound **7** is reasonably stable (unlike its diruthenium analogue), but it underwent photolytic decarbonylation when exposed to ordinary laboratory illumination. The orange-colored product **8** is stable in the atmosphere at 25 °C. So far, no evidence has been obtained that more than two metal atoms can be attached to a cyclotriphosphazene ring or that nongeminal substitution occurs.

An alternative pathway to species **7** and **8** is via a monoiron cyclotriphosphazene (**9**). This compound had not been isolated in the earlier work. However, it has now been found that **2** reacts with 1 equiv of $[Fe(CO)_2Cp]^-$ to form this compound **9** in 5% yield, together with species **3** and **4**, and a considerable amount of $Fe_2(CO)_4Cp_2$. However, surprisingly, the reaction of **9** with $[Ru(CO)_2Cp]^-$ did not yield **7** or **8**. Instead, when a large excess of $[Ru(CO)_2Cp]^-$ was present, the products included $Ru_2(CO)_4Cp_2$ and the red-orange mixed-metal dimer $FeRu(CO)_4Cp_2$ (**10**). This latter compound has not been isolated before. The proof of its structure will be described in a later section.

Compounds **7** and **8** can be compared to species **11** and **12**,

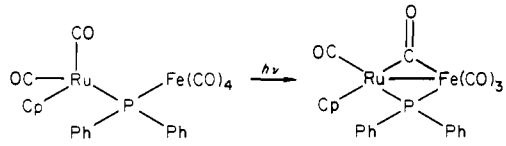

11 12

reported by Haines, DuPreez, and Nolte.[8] Apart from these and the related cations,[8] species **7**, **8**, and **10** appear to be the only mixed-metal Ru–Fe dimeric compounds known at this time.

Reactions of 4, 6, and 8 with Carbon Monoxide. Carbonylation reactions were attempted for three reasons: (1) to determine the stability of the metal–metal-bonded phosphazenes at high temperatures and pressures, (2) to determine if the "nonspiro" derivatives of **4**, **6**, and **8** (i.e., **3**, **7**, or the missing precursor of **6**) could be isolated by this alternative route, and (3) to establish if the new mixed-metal dimer $FeRu(CO)_4Cp_2$ (**10**) is a product from the reaction of **8** with carbon monoxide.

First, it was found that treatment of **6** with carbon monoxide in THF at high pressure (1000 psi) at 110 °C for 5 days did not bring about cleavage of the Ru–Ru bond. Compound **6** was recovered intact. This is an indication of the surprising stability of this species.

By contrast, compound **4** did react with carbon monoxide (at 1200 psi, in THF, at 100 °C for 18 h) to bring about a partial conversion of **4** to **3**. However, the major product was the organometallic iron dimer $Fe_2(CO)_4Cp_2$.

Compound **8** also reacted with carbon monoxide (at 1100 psi, in THF, at 120 °C for 64 h) to give **7**, together with a trace of $Fe_2(CO)_4Cp_2$. No $Ru_2(CO)_4Cp_2$ or $FeRu(CO)_4Cp_2$ were detected.

Explanation of Reaction Anomalies. Four puzzling features of these reactions need to be explained. First, why does the reaction of **5** with $[Ru(CO)_2Cp]^-$ not yield a stable intermediate analogous to **3** or **7**? Second, and related to the first point, why is **6** the only one of the three metal–metal-bonded phosphazenes that does not undergo metal–metal bond cleavage with carbon monoxide? Third, why does **9** fail to react with $[Ru(CO)_2Cp]^-$ to yield **7** and **8**? And fourth, what is the significance of the formation of organometallic dimers such as **10**, $Ru_2(CO)_4Cp_2$, or $Fe_2(CO)_4Cp_2$ in these reactions?

The anomalies surrounding compound **6** can perhaps be explained by the greater strength of the Ru–Ru bond compared to those of the Fe–Fe or Fe–Ru bonds. Bonds between metals of the first transition series are generally weak compared to those between heavier transition metals.[9] Ruthenium–ruthenium bond formation evidently provides a powerful driving force for the formation of **6** even in the absence of light. Moreover, once formed, the bond cannot be disrupted by carbon monoxide. Even when metal–metal bond disruption by carbon monoxide occurs with **4** and **8**, the reaction is not facile. Thus, it must be concluded that the phosphazene ring stabilizes the metal–metal bonds in **4**, **6**, and **8**, perhaps by providing a rigid framework that discourages the conformation changes needed for metal–metal bond cleavage.

We believe that the third and fourth questions mentioned above have a common answer. Compounds **7** and **8** are not formed from **9** because a competing reaction, the formation of **10**, dominates the reaction pathway. Presumably, in this system, the incoming

(8) Haines, R. J.; DuPreez, A. L.; Nolte, C. R. *J. Organomet. Chem.* **1973**, *55*, 199.

(9) Vahrenkamp, H. *Angew. Chem., Int. Ed. Engl.* **1978**, *17*(6), 379.

Scheme I

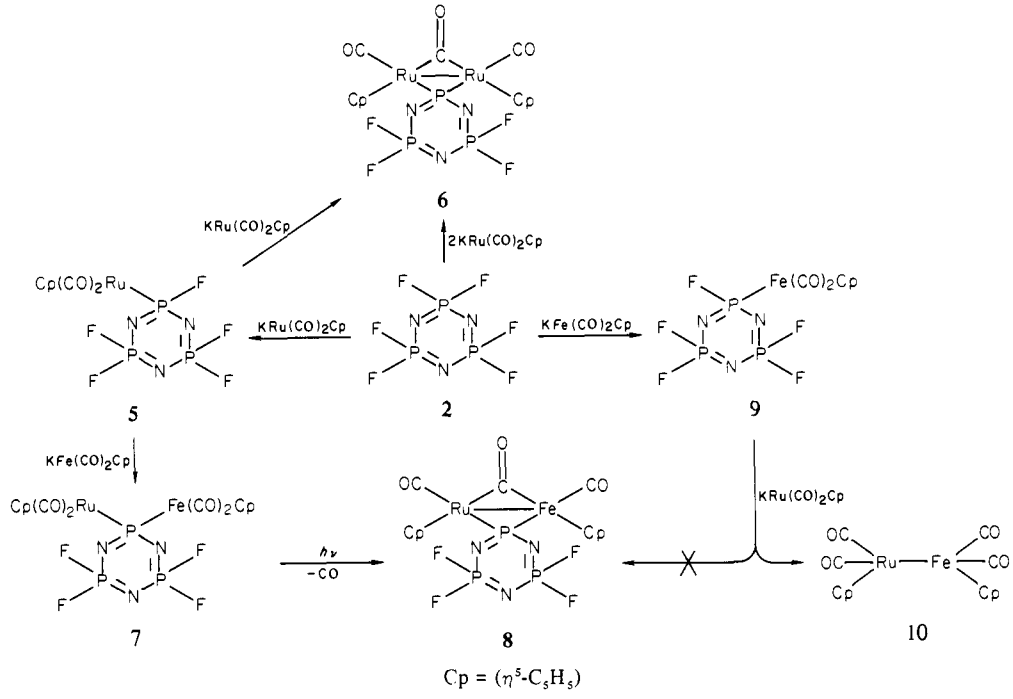

Table I. Infrared and Mass Spectrometric Data

compd	carbonyl stretching frequencies,[a] cm^{-1}	C-H stretch,[c] cm^{-1}	P-N,[c] cm^{-1}	CI mass spectrum	EI (high-resolution) mass spectrum
3[d]	2038 (sh), 2020 (s), 1977 (m, br)	3120	1210, 1240	566 (M_r + 1)	
4[d]	2019 (s), 1984 (m, br), 1805 (s, br)	3120	1220, 1260		
5	2072 (s), 2025 (s)[b]	3120	1100-1300	454 (M_r + 1)	452.8556 (calcd = 452.8551)
6	2019 (s), 1986 (m, br), 1802 (s, br)	3120	1220, 1260	629 (M_r + 1)	628.7916 (calcd = 628.7945)
7	2040 (sh), 2023 (s), 1977 (m, br)	3120	1210, 1240	612 (M_r + 1)	
8	2018 (s), 1985 (m, br), 1802 (s, br)	3120	1220, 1255	584 (M_r + 1)	
9	2058 (s), 2012 (s)	3120	1100-1300	408 (M_r + 1)	406.8843 (calcd = 406.8863)
10	2009 (s), 1961 (s), 1941 (w), 1791 (s)[b]			401 (M_r + 1)	399.8968 (calcd = 399.8971)

[a] CH_2Cl_2 solution. [b] Heptane solution. [c] KBr disk. [d] Reference 3.

anion prefers to attack the metal already present rather than the phosphorus atom (**13**). Species of type **14** would be unstable and would probably undergo skeletal breakdown at 25 °C.

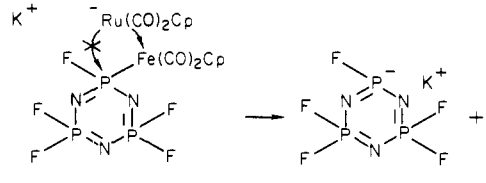

13 **14**

$Cp(CO)_2Ru-Fe(CO)_2Cp$

10

Were it not for the isolation of **10**, it might be assumed that products such as $Fe_2(CO)_4Cp_2$ or $Ru_2(CO)_4Cp_2$ were formed exclusively by oxidation of the respective anions in contact with trace amounts of air in the system.[21] However, the isolation of **10** provides strong evidence that a portion of the dimer formed in these reactions is the result of an attack by the metal anions on species **5** or **9**. Thus, this alternative pathway exists in the formation of compounds **3**, **4**, and **6** (as indicated by the formation of the organometallic dimers), but it appears not to dominate the reaction pathway in these systems, as it apparently does in the reaction of **9** with $[Ru(CO)_2Cp]^-$.

The fact that none of the mixed-metal organometallic dimer **10** was detected when $[Fe(CO)_2Cp]^-$ was allowed to react with **5** suggests that the differences between the reactions of **9** and **5** probably depend on the type of metal atom already attached to phosphorus and on the nucleophilic strength of the incoming anion. If the incoming nucleophile is very strong, such as $[Fe(CO)_2Cp]^-$, attack at the phosphorus atom may be preferred, or at least competitive. If the incoming nucleophile is weaker, such as $[Ru(CO)_2Cp]^-$, attack at the metal center to give the organometallic dimer may be favored.

Spectroscopic Structure Proof for 5–10. The characterization of these compounds made use of mass spectrometry, infrared

(10) Garner, C. D.; Senior, R. G.; King, T. J. *J. Am. Chem. Soc.* **1976**, *98*, 3526.
(11) It was known that the compound was not the diiron analogue (**4**), because its X-ray structure had been determined previously. The cell constants were significantly different from those obtained for **8**. See ref 3.
(12) Gilmore, C. J.; Woodward, P. *J. Chem. Soc. A* **1971**, 3453.
(13) Fox, J. R.; Gladfelter, W. L.; Wood, T. G.; Smegal, J. A.; Foreman, T. K.; Geoffroy, G. L.; Tavanaiepour, I.; Day, V. W.; Day, C. S. *Inorg. Chem.* **1981**, *20*, 3214.
(14) Marsh, W. C.; Ranganathan, T. N.; Trotter, J.; Paddock, N. L. *J. Chem. Soc., Chem. Commun.* **1970**, 815.
(15) Marsh, W. C.; Trotter, J. *J. Chem. Soc. A* **1971**, 573.
(16) Marsh, W. C.; Trotter, J. *J. Chem. Soc. A* **1971**, 569.
(17) Allcock, H. R.; Ritchie, R. J.; Harris, P. J. *Inorg. Chem.* **1980**, *19*, 2483.
(18) Davis, M. I.; Paul, J. W. *Bull. Am. Phys. Soc.* **1968**, *13*, 832.
(19) Lewis, J.; McPartlin, M.; Nelson, W. J. H.; Eady, C. R.; Jackson, P. F.; Johnson, B. F. G.; Malatesta, M. C. *J. Chem. Soc., Dalton Trans.* **1980**, *3*, 383.
(20) Humphries, A. P.; Knox, S. A. R. *J. Chem. Soc., Dalton Trans.* **1975**, 1710.
(21) Ellis, J. E.; Flom, E. A. *J. Organomet. Chem.* **1975**, *99*, 263.
(22) Schmutzler, R. *Inorg. Synth.* **1967**, *9*, 75.

Table II. ^{31}P, ^{19}F, and ^{1}H NMR Data[a]

compd	^{31}P NMR data[b]		^{19}F NMR data[b]	
3[c]	PF_2	−0.3 (t, J_{PF} = 891.4)		
	PFe_2	158.4 (s)		
4[c]	PF_2	3.3 (t, J_{PF} = 918.0)	PF_2	44.7 (d, J_{PF} = 897.0)
	PFe_2	272.3 (s)		
5	PF_2	1.6 (t, J_{PF} = 900.5)	PF_2	44.5 (d, J_{PF} = 903.6)
	PFRu	103.9 (d, J_{PF} = 1117.4)	PFRu	125.0 (d, J_{PF} = 1123.3)
6	PF_2	2.5 (t, J_{PF} = 897.8)	PF_2	44.5 (d, J_{PF} = 893.1)
	PRu_2	229.9 (s)		
7	PF_2	−1.5 (t, J_{PF} = 888.8)	PF_2	43.6 (d, J_{PF} = 890.6)
	PFeRu	126.1 (s)		
8	PF_2	2.3 (t, J_{PF} = 916.9)	PF_2	44.6 (d, J_{PF} = 880.1)
	PFeRu	249.7 (s)		
9	PF_2	1.4 (t, J_{PF} = 920.0)	PF_2	44.2 (d, J_{PF} = 919.0)
	PFFe	133.2 (d, J_{PF} = 1141.2)	PFFe	122.2 (d, J_{PF} = 1145.4)

[a] ^{1}H NMR data in $CDCl_3$ solution are as follows (with chemical shifts in ppm in parentheses): 3 (5.3), 4 (4.9), 5 (5.5), 6 (5.3), 7 (4.98, 5.47), 8 (4.83, 5.33), 9 (5.1), 10 (4.79, 5.29). [b] Chemical shifts in ppm and coupling constants in hertz. [c] Reference 3.

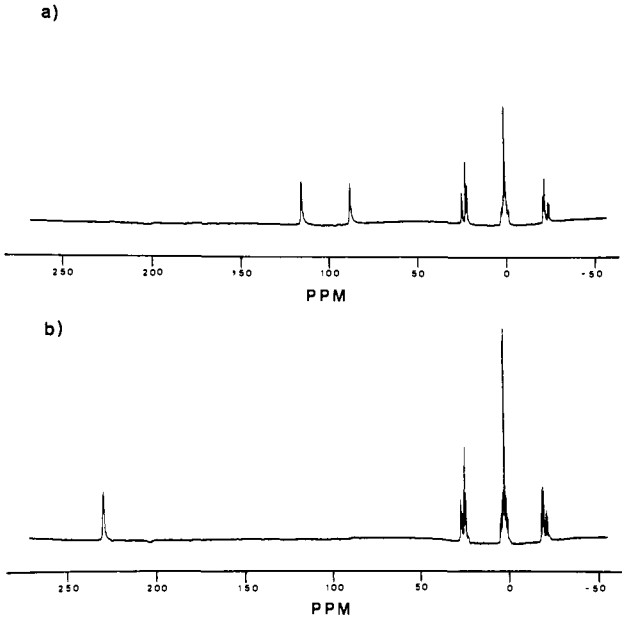

Figure 1. The ^{31}P NMR spectra (proton decoupled) of (a) $N_3P_3F_5Ru(CO)_2Cp$ (**5**) and (b) $N_3P_3F_4Ru_2(CO)_3Cp_2$ (**6**).

spectroscopy, and ^{1}H, ^{19}F, and ^{31}P NMR data.[23] These data are summarized in Tables I and II, and the following is illustrative of the general techniques employed.

The structure of **5** was deduced in the following way. The chemical ionization (CI) mass spectrum of **5** contained a peak at 454 amu (M_r + 1), and the high-resolution electron impact spectrum suggested a M_r of 452.8556 (calcd = 452.8551). The infrared spectrum of **5** in heptane showed strong carbonyl absorbances at 2072 and 2025 cm^{-1}, plus characteristic absorbances for P–N bonds between 1100 and 1300 cm^{-1} and a C–H stretch at 3120 cm^{-1}. The ^{1}H NMR spectrum of **5** consisted of a singlet at 5.5 ppm. The ^{19}F NMR spectrum consisted of two doublets (PF_2 δ^F 44.5, J_{PF} = 903.6 Hz; PFRu δ^F 125.0, J_{PF} = 1123.3 Hz). The ^{31}P NMR spectrum consisted of a major triplet (PF_2 δ^P 1.6, J_{PF} = 900.5 Hz) and a doublet (PFRu δ^P 103.9, J_{PF} = 1117.4 Hz). All these data are consistent with structure **5**.

The structures of **6–9** were determined in a similar way (Tables I and II). In general, marked similarities were detected between the infrared and NMR spectra of **5** and **9**, **3** and **7**, and **4**, **6**, and **8**. Representative ^{31}P NMR spectra are given for **5** and **6** in Figure 1. In addition, the structure of **8** was confirmed by X-ray crystallography (see later).

(23) ^{1}H NMR chemical shifts were referenced to Me_4Si, ^{19}F NMR chemical shifts to monofluorobenzene in $CDCl_3$, and ^{31}P NMR chemical shifts to aqueous H_3PO_4. In all cases, positive chemical shifts are downfield from the reference. The PF_2 component of the ^{19}F and ^{31}P NMR spectra was complicated by second-order effects.

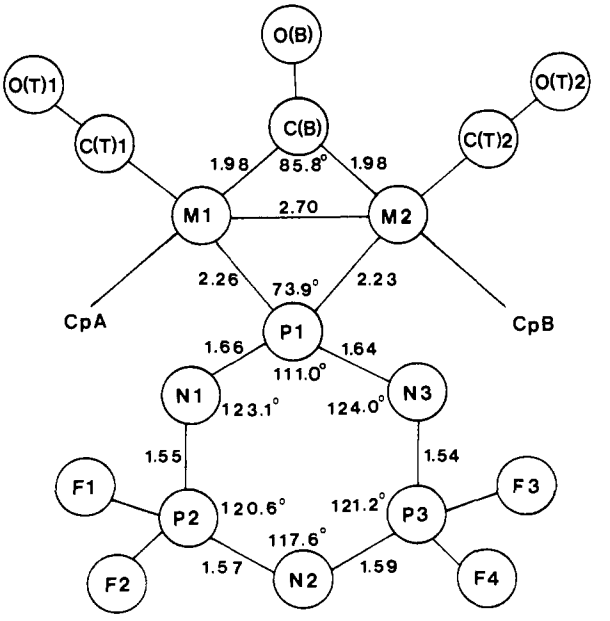

M1 = 0.5 Fe1 + 0.5 Ru2
M2 = 0.5 Fe2 + 0.5 Ru1

Figure 2. Representation of the structure of **8**, showing specific bond angles and interatomic distances.

The identity of $FeRu(CO)_4Cp_2$ (**10**) was deduced in the following way. The CI mass spectrum contained a peak at 401 (M_r + 1), and the EI mass spectrum showed a parent peak at m/e 400 with the successive loss of four carbonyl groups (m/e −28) at 372, 344, 316, and 288. The correct isotope pattern for $FeRu(CO)_4Cp_2$ was obtained in both cases. The high-resolution electron impact mass spectrum suggested a M_r of 399.8968 (calcd = 399.8971). The 200-MHz ^{1}H NMR spectrum of **10** consisted of two peaks of equal area, one arising from the cyclopentadienyl group attached to iron (4.79 ppm), and the other from the cyclopentadienyl group attached to ruthenium (5.29 ppm). These chemical shifts are compatible with the values found for the two homonuclear dimers. The infrared spectrum of **10** in heptane showed carbonyl absorbances at 2009 (s), 1961 (s), 1941 (w), and 1791 (s) cm^{-1}.

The mixed-metal dimer appeared to disproportionate to $Fe_2(CO)_4Cp_2$ and $Ru_2(CO)_4Cp_2$ when heated. Species **10** was also synthesized independently by the interaction of one equivalent each of $[Ru(CO)_2Cp]^-$ and $Fe(CO)_2CpI$. To our knowledge, this is the first reported isolation of **10**.

X-ray Analysis of 8. The X-ray structure analysis of **8** revealed that the molecule contains the expected geminal disposition of

the two metals and the presence of the metal–metal bond and the carbonyl bridge. All features of the molecule were identified. The principal structural parameters are summarized in Figure 2. A stereoview showing the general molecular geometry is available as supplementary material.

The two metal atoms were statistically disordered on their sites. This type of disorder is not unexpected and has been observed elsewhere.[10] Thus, in the absence of alternative data, the Patterson map could also be consistent with structure **6** rather than **8**.[11] However, this interpretation was ruled out on the basis of the general analytical data and by the use of CI mass spectrometry to show that the crystal used for the X-ray data collection was indeed that of compound **8**.

The coordination geometry about the metal atoms in **8** is as follows: The iron and ruthenium atoms are separated by a distance of 2.698 Å. This suggests the presence of an Fe–Ru bond, since the value is ≃0.1 Å longer than that found in **4**[3] and is of similar length to the Fe–Ru bonds in other compounds.[12,13] The average metal–phosphorus bond distance of 2.24 Å and the metal–phosphorus–metal bond angle of 73.9° are slightly larger than the values found in **4**.[3]

The two η^5-cyclopentadienyl ligands were cis to each other, relative to the metal–metal bond. This also corresponds to the structure found for **4**.[3] At this time, no mechanistic significance is attached to the cis geometry. The predominance of one isomer may simply reflect a nuance of the crystallization technique. The cyclopentadiene rings are planar and are separated from the metal atoms by an average metal–carbon distance of 2.18 Å. The average metal to terminal carbonyl carbon distance is 1.84 Å, and the corresponding distance to the bridging carbonyl carbon is 1.98 Å. As expected, the C–O distance of the bridging carbonyl (1.175 Å) is slightly longer than the average for the terminal carbonyl ligands (1.15 Å).

Within the phosphazene ring the two P–N bonds proximal to the metal atoms were the longest in length (mean distance of 1.65 Å). The adjacent pair of P–N bonds were the shortest (mean distance 1.55 Å), and those furthest from the metal atoms were of intermediate length (1.58 Å). This pattern of bond length variation has been observed in other asymmetrically substituted cyclophosphazenes.[3,14-17] The remaining structural features of **8** are similar to those of **4**[3] and to those of **2**.[18] The organometallic unit exerts its greatest influence on the phosphazene ring in the immediate environment of the phosphorus–metal bonds.

Experimental Section

Materials. $Fe_2(CO)_4Cp_2$ and $Ru_3(CO)_{12}$ were obtained from Alfa or Strem Chemicals, Inc., and were used as received. $Ru_3(CO)_{12}$ was also prepared by the high-pressure carbonylation[19] of $RuCl_3 \cdot 3H_2O$ (Alfa). Cyclopentadiene was prepared by the thermal cracking of dicyclopentadiene (Aldrich). $Ru_2(CO)_4Cp_2$ was synthesized from $Ru_3(CO)_{12}$ and cyclopentadiene.[20] Sodium–potassium alloy (NaK)[21] was prepared from sodium and potassium metals (Fisher). Hexachlorocyclotriphosphazene $(NPCl_2)_3$ (Ethyl Corp.), sublimed and recrystallized twice from hexane, and sodium fluoride (Fisher) were used to synthesize $(NPF_2)_3$ by an established procedure.[22] Tetrahydrofuran (Baker) was dried and distilled from sodium benzophenone ketyl. Methylene chloride, hexane, and toluene were obtained from Baker Chemical Co. Heptane and xylene (Baker) were dried over calcium hydride. Hi-Flosil (60–200 mesh) (Applied Science Laboratories, Inc.) and Silica Gel 60 (0.040–0.063 mm, 230–400 mesh ASTM) (Scientific Products) were used as received.

All reactions were carried out under an atmosphere of nitrogen in standard Schlenk glassware.

Analytical Equipment. Infrared spectra were recorded on a Perkin-Elmer Model 580 grating spectrophotometer. ^{31}P and ^{19}F NMR spectra[23] were obtained with the use of a Jeol PS-100 FT NMR spectrometer. ^1H NMR spectra[23] were obtained with the use of a Varian EM 360 spectrometer or a Bruker WH 200 Fourier transform spectrometer. Chemical ionization mass spectra were obtained with the use of a Finnigan 3200 mass spectrometer, using methane or isobutane as the ionizing gas. High-resolution electron impact mass spectra were obtained with the use of an AEI MS-902 mass spectrometer.

Synthesis of (1,3,3,5,5-Pentafluorocyclotriphosph(P^V)azen-1-yl)dicarbonylcyclopentadienylruthenium (5). To a solution of $Ru_2(CO)_4Cp_2$ (3.10 g, 6.98 mmol) in dry THF (175 mL) was added NaK alloy (1–2 mL) via syringe. The reaction mixture was stirred at 25 °C for approximately 4 h. During this time a color change was observed. The infrared spectrum of the mixture contained two very broad carbonyl absorbances between 1759–1900 cm^{-1}, indicative of the formation of the $[Ru(CO)_2Cp]^-$ anion. The anion solution was then transferred to a coarse-fritted addition funnel and was added dropwise to a solution of $(NPF_2)_3$ (2.32 g, 9.30 mmol) in dry THF (25 mL). The reaction mixture was then stirred at 25 °C for 48 h.

The THF was removed from the reaction mixture with the use of a rotary evaporator. The residue was then extracted with CH_2Cl_2 (250 mL). After removal of the CH_2Cl_2 by rotary evaporation, the extracted solids were chromatographed with a column packed with Hi-flosil silica gel as a slurry in hexane. Elution with a 25% CH_2Cl_2/75% hexane solvent mixture removed a yellow-orange band from the column. This was found to be $Ru_2(CO)_4Cp_2$ on the basis of its infrared spectrum. Further elution with 50% CH_2Cl_2/50% hexane yielded a colorless fraction that contained **5**. Removal of the solvent gave **5** as a white solid (mp 81–83 °C) in approximately 15% yield. The high-resolution mass spectrum was consistent with the formula $C_7H_5O_2N_3F_5P_3Ru$. Other characterization data are summarized in Tables I and II.

Synthesis of (μ-Carbonyl)(μ-3,3,5,5-tetrafluorocyclotriphosph(P^V)azene-1,1-diyl)bis(carbonylcyclopentadienylruthenium) (*Ru–Ru*) (6). This compound could be prepared by two different routes—from **5** or from $(NPF_2)_3$ (**2**). These methods are described in turn.

To a solution of $Ru_2(CO)_4Cp_2$ (0.38 g, 0.86 mmol) in dry THF (100 mL) was added NaK alloy (1–2 mL) via syringe. The reaction mixture was stirred at 25 °C for 3.5 h. The $[Ru(CO)_2Cp]^-$ solution was then transferred to a coarse-fritted addition funnel and was added dropwise to a solution of **5** (0.53 g, 1.17 mmol) in dry THF (25 mL). The reaction mixture was then stirred at 25 °C for 48 h. The THF was removed from the reaction mixture with the use of a rotary evaporator. The crude solids were then extracted with CH_2Cl_2 (100 mL), and the CH_2Cl_2 was removed by rotary evaporation. The remaining solid residue was dissolved in a minimum amount of a 50% CH_2Cl_2/50% hexane solvent mixture and was introduced onto a column packed with Silica Gel 60 (column height 6 in.) in a 25% CH_2Cl_2/75% hexane mixture. Elution with the same solvent mixture (under a slight nitrogen pressure) removed a yellow-orange band from the column. This contained $Ru_2(CO)_4Cp_2$ (identified by IR spectroscopy). A yellow band was then eluted by increasing the CH_2Cl_2 concentration in the eluant first to 50% and then to 100%. This fraction contained a mixture of **5** and **6** (identified by ^{31}P NMR and IR techniques). The two compounds were separated by fractional sublimation. At 30 °C and 0.1 torr, compound **5** sublimed onto the cold finger leaving the pure yellow **6** behind. The yield of **6** was 10% (mp 200 °C dec). High-resolution mass spectrometry data were compatible with the formula $C_{13}H_{10}O_3N_3F_4P_3Ru_2$.

The alternative route is as follows: To a solution of $Ru_2(CO)_4Cp_2$ (3.00 g, 6.75 mmol) in dry THF (150 mL) was added NaK alloy (1–2 mL) via syringe. The reaction mixture was stirred at 25 °C for 4.5 h. The $[Ru(CO)_2Cp]^-$ solution was then transferred to a coarse-fritted addition funnel and was added dropwise to a solution of $(NPF_2)_3$ (1.11 g, 4.46 mmol) in dry THF (50 mL). The reaction mixture was stirred at 25 °C for 72 h. The reaction mixture contained $Ru_2(CO)_4Cp_2$ (identified by IR spectroscopy) and compounds **5** and **6** (identified by ^{31}P NMR spectrometry). Compound **6** was isolated as described above.

Synthesis of (1,3,3,5,5-Pentafluorocyclotriphosph(P^V)azen-1-yl)dicarbonylcyclopentadienyliron (9). To a solution of $Fe_2(CO)_4Cp_2$ (1.42 g, 4.03 mmol) in dry THF (150 mL) was added NaK alloy (1–2 mL) via syringe. The reaction mixture was stirred at 25 °C for 2.5 h. The $[Fe(CO)_2Cp]^-$ solution was then transferred to a coarse-fritted addition funnel and was added dropwise to a solution of $(NPF_2)_3$ (2.04 g, 8.20 mmol) in dry THF (40 mL). The reaction mixture was stirred at 25 °C for 48 h. The THF was removed from the reaction mixture with the use of a rotary evaporator. The solid residue was then dissolved in CH_2Cl_2 (100 mL) and the solution was passed down a short, wide silica gel column. The CH_2Cl_2 was removed by rotary evaporation. The residual solid was then dissolved in a minimum amount of CH_2Cl_2 and the solution was chromatographed over Hi-Flosil silica gel as a hexane slurry. Elution with a 20% CH_2Cl_2/80% hexane solvent mixture removed a dark red band from the column. This was identified as $Fe_2(CO)_4Cp_2$ on the basis of its infrared spectrum and by mass spectrometry. Compounds **9** and **4** were removed from the column as a light red band by elution with a 50% CH_2Cl_2/50% hexane mixture. Compound **3** was removed from the column as a bright yellow band by elution with 100% CH_2Cl_2. Compound **3** was eventually transformed to **4** on exposure to room light. Compound **9** was separated from **4** by fractional sublimation. At 25 °C and 0.1 torr, **9** sublimed onto the cold finger leaving the red compound **4** as a residue. Compound **9** was isolated as a very pale yellow crystalline solid: yield 5%; mp 107–109 °C. High-resolution mass spectrometry data were compatible with the formula $C_7H_5O_2N_3F_5P_3Fe$.

Synthesis of [1-(Dicarbonylcyclopentadienylruthenium-σ-3,3,5,5-tetrafluorocyclotriphosph(P^V)azen-1-yl)dicarbonylcyclopentadienyliron (7) and (μ-Carbonyl)(μ-3,3,5,5-tetrafluorocyclotriphosphazene-1,1-diyl)-(carbonylcyclopentadienylruthenium)carbonylcyclopentadienyliron(*Ru-Fe*) (8). To a solution of $Fe_2(CO)_4Cp_2$ (0.30 g, 0.84 mmol) in dry THF (100 mL) was added NaK alloy (1–2 mL) via syringe. The reaction mixture was stirred at 25 °C for 2 h. The $[Fe(CO)_2Cp]^-$ solution was then transferred to a coarse-fritted addition funnel and was added dropwise to a solution of **5** (0.50 g, 1.10 mmol) in dry THF (75 mL). The reaction mixture was stirred at 25 °C, in the absence of light for 48 h. The THF was removed from the reaction mixture with the use of a rotary evaporator. The crude solids were then extracted with CH_2Cl_2 (100 mL) and the CH_2Cl_2 was removed by rotary evaporation. The solid residue was dissolved in a minimum amount of a 50% CH_2Cl_2/50% hexane mixture and was column chromatographed over Hi-Flosil in hexane. A dark red band, $Fe_2(CO)_4Cp_2$ (identified by infrared spectroscopy), and an orange band (a mixture of compounds **5** and **8** identified by ^{31}P NMR spectroscopy) were removed from the column by elution initially with a 10% CH_2Cl_2/90% hexane solvent mixture, followed by a 40% CH_2Cl_2/60% hexane solvent mixture. A bright yellow band, **7**, was eluted cleanly with 100% CH_2Cl_2. Chromatography (Hi-Flosil) with toluene as the eluant resulted in the separation of compounds **5** and **8**, to give the orange-colored **8** in low yield. Compound **8** can also be prepared in high yield from **7** by exposure to room light. Compounds **7** and **8** are crystalline solids. They do not have clean melting points but decompose at temperatures above 175 °C.

Synthesis of $FeRu(CO)_4Cp_2$ (10). The interaction of **9** with $[Ru(CO)_2Cp]^-$ in THF at 25 °C in the dark yielded only unchanged **9** and $Ru_2(CO)_4Cp_2$ when the ratio of the two reactants was 1:1.5 or 1:3.5. Only when a larger excess of $[Ru(CO)_2Cp]^-$ was used did a significant reaction occur. Thus, NaK alloy (1–2 mL) was added by syringe to a solution of $Ru_2(CO)_4Cp_2$ (2.56 g, 5.75 mmol) in dry THF (80 mL). The reaction mixture was stirred at 25 °C for 3 h and the solution was then added dropwise through a coarse-fritted funnel to a solution of **9** (0.71 g, 1.73 mmol) in THF (30 mL). After reaction at 25 °C for 72 h with the mixture shielded from light, the THF was removed by means of a rotary evaporator. The solid residue was dissolved in a minimum amount of CH_2Cl_2 and was chromatographed over Hi-Flosil. A red band and a yellow-orange band were removed from the column by elution with a 25% CH_2Cl_2/75% hexane mixture initially, followed by a 50% CH_2Cl_2/50% hexane mixture. The yellow-orange band contained $Ru_2(CO)_4Cp_2$ (detected by IR and mass spectral analyses). The red band contained a mixture of $FeRu(CO)_4Cp_2$ and $Ru_2(CO)_4Cp_2$. These two compounds were separated by column chromatography using a column packed with Silica Gel 60 (column height 6 in.) as a hexane slurry, with elution with a CH_2Cl_2–hexane solvent mixture having a CH_2Cl_2 composition of no greater than 20%, under a slight pressure of nitrogen. The $Ru_2(CO)_4Cp_2$ moved down the column first, followed by the $FeRu(CO)_4Cp_2$. Removal of the solvent under vacuum resulted in the isolation of the red-orange, crystalline $FeRu(CO)_4Cp_2$ (**10**). High-resolution mass spectrometry data were compatible with the formula $C_{14}H_{10}O_4FeRu$.

Alternatively, compound **10** could be synthesized by allowing 1 equiv of $[Ru(CO)_2Cp]^-$ to react with $Fe(CO)_2CpI$. To a solution of $Ru_2(CO)_4Cp_2$ (1.9 g, 4.3 mmol) in dry THF (~150 mL) was added NaK alloy (1–2 mL) via syringe. The $[Ru(CO)_2Cp]^-$ solution was then transferred to a coarse-fritted addition funnel and was added dropwise to a solution of $Fe(CO)_2CpI$ (2.6 g, 8.5 mmol) in dry THF (~50 mL) at −78 °C. The reaction mixture was allowed to warm to room temperature and was then stirred at room temperature overnight.

The THF was removed from the reaction mixture with the use of a rotary evaporator. The solid residue was dissolved in a minimum amount of CH_2Cl_2 and was column chromatographed over Hi-Flosil in hexane. Elution with 25% CH_2Cl_2/75% hexane resulted in the removal of a brown band from the column (a mixture of $Fe(CO)_2CpI$ and $Ru_2(CO)_4Cp_2$ as identified by IR and CI mass spectral data). Elution with a CH_2Cl_2–hexane solvent mixture, having a composition of 50% CH_2Cl_2 or greater, resulted in the removal of a red-orange band from the column. This band contained a mixture of $FeRu(CO)_4Cp_2$ and $Ru_2(CO)_4Cp_2$ (as identified from CI mass spectral and ^1H NMR data). These two compounds were separated by column chromatography in a manner identical with that outlined above.

Reactions of Compound 6 with Carbon Monoxide. (1) A pressure bomb was charged with 50–100 mg of compound **6** dissolved in 20 mL of dry THF. The bomb was pressurized to 600 psi with CO and was heated at 60 °C for 18 h. (2) A pressure bomb was charged with 50–100 mg of compound **6** dissolved in 20 mL of dry THF. The bomb was pressurized to 1200 psi with CO and was heated at 100 °C for 18 h. (3) A pressure bomb was charged with approximately 250 mg of compound **6** dissolved in 20 mL of dry THF. The bomb was pressurized to 1000 psi with CO and was heated at 110 °C for 5 days.

Reactions of Compound 4 with Carbon Monoxide. The carbonylation reactions were carried out under two different sets of conditions. These conditions were identical with those given in (1) and (2) above.

Reactions of Compound 8 with Carbon Monoxide. (1) A pressure bomb was charged with 50–100 mg of compound **8** dissolved in 20 mL of dry THF. The bomb was pressurized to 640 psi with CO and was heated at 60 °C for 16 h. (2) A pressure bomb was charged with 50–100 mg of compound **8** dissolved in 20 mL of dry THF. The bomb was pressurized to 1200 psi with CO and was heated at 100 °C for 22 h. (3) A pressure bomb was charged with 50–100 mg of compound **8** dissolved in 20 mL of dry THF. The bomb was pressurized to 1100 psi with CO and was heated at 120 °C for 64 h.

In all cases, the solutions were cooled to room temperature in the bomb under high carbon monoxide pressure before analysis of the products. If it was evident that a reaction had taken place (as determined by IR and ^{31}P NMR analyses of the crude reaction mixtures), the products were isolated by column chromatography using Hi-Flosil and CH_2Cl_2–hexane solvent mixtures as eluents.

Single-Crystal X-ray Data Collection for 8. Compound **8** crystallized from chloroform as orange prismatic crystals. A crystal with dimensions ca. 0.30 × 0.15 × 1.0 mm was mounted on a glass fiber along the longer axis. The crystal was mounted in a random orientation on an Enraf-Nonius CAD-IV diffractometer, and 25 reflections were located and centered. A least-squares refinement of the 2θ values for these 25 reflections indicated a triclinic lattice with the unit cell dimensions: a = 9.256 (2) Å, b = 14.302 (3) Å, c = 7.975 (16) Å, α = 91.10 (7)°, β = 113.82 (6)°, γ = 93.11 (2)°, and V = 963.4 Å^3. The volume is consistent with $Z = 2$ for a $\rho_{calcd} \simeq 2.0$ g/cm^3. An application of the zero-moment test of Howells, Phillips, and Rodgers[24] indicated a centrosymmetric cell and therefore suggested the space group $P\bar{1}$.

The diffractometer was equipped with a molybdenum X-ray tube (λ_α = 0.71073 Å), operated at 45 kV and 20 mA, and with a graphite-crystal incident-beam monochromator. The crystal to incident-beam collimator distance was 48 mm, and the crystal to aperture distance was 17.3 cm. The takeoff angle was 2.80°. A $\theta/2\theta$ scan technique was used for all reflections for which $0.01° \le 2\theta \le 60°$ with a variable scan rate ranging from 20 deg/min for the most intense reflections to 1 deg/min for the weaker reflections. The angular scan width was determined from the equation $\Delta\theta = (0.6 + 0.347 \tan\theta)°$ and was extended by 25% on each side of the scan range for measurement of background intensities. During the data collection, three standard reflections were monitored after every 4 h of actual X-ray exposure time. The standard reflections were used to correct the observed structure factor amplitudes and its standard deviation for anisotropic decay of the crystal with time. The correction factors were obtained by interpolating between each set of standard reflections after having corrected those standards to zero time. The correction factors varied from 1.140 to 0.979 with an average value of 1.059. This variation was random and long term.

From a total of 5985 unique reflections collected, 4403 were considered observed with $I \ge 2\sigma(I)$. The net intensity, I, and the standard deviation, $\sigma(I)$, were calculated from $I = S(C - RB)$ and $\sigma(I) = [S^2(C + R^2B) + (\kappa I)^2]^{1/2}$, where S is the scan rate, C is the total integrated peak count, R is the ratio of scan time to background counting time, B is the total background count, and κ, a factor to downweight intense reflections, was set equal to 0.02. Lorentz and polarization corrections were applied in the determination of structure amplitudes.[25] The linear absorption coefficient, μ, was calculated to be 18.40 cm^{-1} and no absorption correction was applied.

Structure Determination and Refinement. An origin-removed Patterson map revealed the positions of the iron and ruthenium atoms and the three phosphorus atoms. It also indicated that an equal amount of electron density occupied each of the two metal atom positions due to a statistical disorder of the metal atoms on their sites. Each metal site was considered to be occupied by 0.5 Ru and 0.5 Fe atoms. Full-matrix least-squares refinement was accomplished by refining the parameters of the ruthenium atoms and setting the parameters of the iron atoms equal to those of the ruthenium atoms. Three cycles of refinement of the positional and isotropic thermal parameters of the metal and the phosphorus atoms resulted in R_1 = 0.311 and R_2 = 0.356.[26] Subsequent Fourier and difference maps located the remaining non-hydrogen atoms. Refinement on positional and anisotropic thermal parameters for the

(24) Howells, E. R.; Phillips, D. C.; Rogers, D. *Acta Crystallogr.* **1950**, *3*, 210.

(25) All the programs used in the refinement were part of the Enraf-Nonius structure determination package (SPD), Enraf-Nonius, Delft, Holland, 1975, revised 1977, and implemented on a PDP 11/34 computer.

(26) $R_1 = \sum||F_o| - |F_c||/\sum|F_o|$ and $R_2 = [\sum w(|F_o| - |F_c|)^2/\sum w(F_o)^2]^{1/2}$, where $w = 1/(\sigma(F_o))^2$. The function minimized was $\sum w(|F_o| - |F_c|)^2$, where $\sigma(F_o)^2 = [\sigma(I)^2 + (0.02F^2)^2]^{1/2}/(Lp)$ and $F_o^2 = F^2/(Lp)$.

Table III. Distances and Angles in $[N_3P_3F_4FeRu(\eta^5\text{-}C_5H_5)_2(CO)_3]$ (8)

	Distances, Å		
Ru(1)-Fe(1)	2.698 (1)	P(3)-F(3)	1.529 (2)
Ru(1)-P(1)	2.231 (1)	P(3)-F(4)	1.556 (2)
Ru(1)-CB	1.983 (2)	OB-CB	1.175 (3)
Ru(1)-CT(2)	1.834 (4)	OT(1)-CT(1)	1.134 (3)
Ru(1)-Cp(1B)	2.200 (3)	OT(2)-CT(2)	1.167 (5)
Ru(1)-Cp(2B)	2.170 (4)	Cp(1A)-Cp(2A)	1.419 (5)
Ru(1)-Cp(3B)	2.140 (4)	Cp(2A)-Cp(3A)	1.373 (5)
Ru(1)-Cp(4B)	2.148 (3)	Cp(3A)-Cp(4A)	1.399 (5)
Ru(1)-Cp(5B)	2.187 (3)	Cp(4A)-Cp(5A)	1.406 (5)
Fe(1)-P(1)	2.256 (1)	Cp(5A)-Cp(1A)	1.398 (5)
Fe(1)-CB	1.980 (3)	Cp(1B)-Cp(2B)	1.385 (6)
Fe(1)-CT(1)	1.847 (3)	Cp(2B)-Cp(3B)	1.391 (8)
Fe(1)-Cp(1A)	2.220 (3)	Cp(3B)-Cp(4B)	1.377 (7)
Fe(1)-Cp(2A)	2.207 (3)	Cp(4B)-Cp(5B)	1.343 (7)
Fe(1)-Cp(3A)	2.160 (3)	Cp(5B)-Cp(1B)	1.383 (5)
Fe(1)-Cp(4A)	2.175 (3)	Cp(1A)-H(1A)	0.92 (3)
Fe(1)-Cp(5A)	2.229 (3)	Cp(2A)-H(2A)	0.90 (3)
P(1)-N(1)	1.656 (2)	Cp(3A)-H(3A)	1.02 (3)
P(1)-N(3)	1.642 (2)	Cp(4A)-H(4A)	1.05 (3)
P(2)-N(1)	1.552 (2)	Cp(5A)-H(5A)	1.01 (3)
P(2)-N(2)	1.574 (2)	Cp(1B)-H(1B)	1.02 (3)
P(2)-F(1)	1.551 (2)	Cp(2B)-H(2B)	0.66 (3)
P(2)-F(2)	1.535 (2)	Cp(3B)-H(3B)	0.78 (3)
P(3)-N(2)	1.589 (2)	Cp(4B)-H(4B)	0.91 (3)
P(3)-N(3)	1.542 (2)	Cp(5B)-H(5B)	0.87 (3)
	Angles, deg		
Ru(1)-P(1)-Fe(1)	73.93 (2)	Cp(5A)-Cp(1A)-Cp(2A)	108.0 (3)
P(1)-Ru(1)-Fe(1)	53.46 (2)	Cp(1A)-Cp(2A)-Cp(3A)	107.7 (3)
P(1)-Fe(1)-Ru(1)	52.61 (2)	Cp(2A)-Cp(3A)-Cp(4A)	109.0 (3)
Ru(1)-CB-Fe(1)	85.82 (9)	Cp(3A)-Cp(4A)-Cp(5A)	108.0 (3)
CB-Ru(1)-Fe(1)	47.04 (8)	Cp(4A)-Cp(5A)-Cp(1A)	107.3 (3)
CB-Fe(1)-Ru(1)	47.15 (7)	Cp(5B)-Cp(1B)-Cp(2B)	106.0 (4)
Ru(1)-CB-OB	136.8 (2)	Cp(1B)-Cp(2B)-Cp(3B)	108.7 (4)
Fe(1)-CB-OB	137.3 (2)	Cp(2B)-Cp(3B)-Cp(4B)	106.6 (4)
Ru(1)-CT(2)-OT(2)	177.7 (3)	Cp(3B)-Cp(4B)-Cp(5B)	109.0 (4)
Fe(1)-CT(1)-OT(1)	175.2 (3)	Cp(4B)-Cp(5B)-Cp(1B)	109.7 (4)
Ru(1)-P(1)-N(1)	118.75 (8)	H(1A)-Cp(1A)-Cp(5A)	129 (2)
Fe(1)-P(1)-N(1)	116.64 (8)	H(1A)-Cp(1A)-Cp(2A)	122 (2)
Ru(1)-P(1)-N(3)	115.39 (8)	H(2A)-Cp(2A)-Cp(1A)	118 (2)
Fe(1)-P(1)-N(3)	116.93 (9)	H(2A)-Cp(2A)-Cp(3A)	134 (2)
N(1)-P(1)-N(3)	111.0 (1)	H(3A)-Cp(3A)-Cp(2A)	122 (2)
N(1)-P(2)-N(2)	120.6 (1)	H(3A)-Cp(3A)-Cp(4A)	129 (2)
N(2)-P(3)-N(3)	121.2 (1)	H(4A)-Cp(4A)-Cp(3A)	118 (2)
P(1)-N(1)-P(2)	123.1 (1)	H(4A)-Cp(4A)-Cp(5A)	134 (2)
P(2)-N(2)-P(3)	117.6 (1)	H(5A)-Cp(5A)-Cp(4A)	139 (2)
P(1)-N(3)-P(3)	124.0 (1)	H(5A)-Cp(5A)-Cp(1A)	114 (2)
F(1)-P(2)-F(2)	96.5 (1)	H(1B)-Cp(1B)-Cp(5B)	127 (2)
F(3)-P(3)-F(4)	95.6 (1)	H(1B)-Cp(1B)-Cp(2B)	126 (2)
N(1)-P(2)-F(1)	109.2 (1)	H(2B)-Cp(2B)-Cp(1B)	131 (3)
N(2)-P(2)-F(1)	108.9 (1)	H(2B)-Cp(2B)-Cp(3B)	120 (3)
N(1)-P(2)-F(2)	111.0 (1)	H(3B)-Cp(3B)-Cp(2B)	118 (3)
N(2)-P(2)-F(2)	108.0 (1)	H(3B)-Cp(3B)-Cp(4B)	135 (3)
N(2)-P(3)-F(3)	107.4 (1)	H(4B)-Cp(4B)-Cp(3B)	124 (2)
N(3)-P(3)-F(3)	111.3 (1)	H(4B)-Cp(4B)-Cp(5B)	127 (2)
N(2)-P(3)-F(4)	109.3 (1)	H(5B)-Cp(5B)-Cp(4B)	131 (2)
N(3)-P(3)-F(4)	109.1 (1)	H(5B)-Cp(5B)-Cp(1B)	119 (2)

non-hydrogen atoms gave $R_1 = 0.057$ and $R_2 = 0.070$. The hydrogen atoms were located by a difference Fourier synthesis. Isotropic thermal parameters for the hydrogen atoms were set at $B = 5.0$ Å^2. Least-squares refinement on all positional parameters, and anisotropic thermal parameters for non-hydrogen atoms, resulted in convergence and yielded $R_1 = 0.056$ and $R_2 = 0.068$ with an esd of an observation of unit weight = 3.658. In the final cycle the largest parameter shift was 0.07 times the esd. A final difference map was featureless and revealed no electron density greater than 0.53 e/Å^3. The atomic scattering factors used for all atoms were those of Cromer and Waber.[27] Anomalous dispersion corrections[27] (both real and imaginary parts) were applied.

Interatomic distances and angles with esd's are listed in Table III. Tables of least-squares planes and interplanar angles, observed and calculated structure factor amplitudes, positional and thermal parameters from the final cycle of refinement (Tables IV–VI), and a stereoview of the molecular geometry of **8** are available as supplementary material.

(27) Cromer, D. T.; Waber, J. T. "International Tables for X-ray Crystallography"; Kynoch Press: Birmingham, England, 1974; Vol. IV, Tables 2.2B and 2.3.1.

Acknowledgment. This work was supported by the U.S. Army Research Office. We thank R. Minard, P. Suszko, and R. Nissan for mass spectral and NMR data, R. Whittle for helpful discussions concerning the X-ray study, and G. Riding and R. Rosen for help with some of the synthetic procedures.

Registry No. 2, 15599-91-4; **4**, 70538-16-8; **5**, 84303-17-3; **6**, 84303-18-4; **7**, 84303-19-5; **8**, 84303-20-8; **9**, 84303-21-9; **10**, 84280-02-4; Fe, 7439-89-6; Ru, 7440-18-8.

Supplementary Material Available: Listing of least-squares planes and interplanar angles, observed and calculated structure factor amplitudes, positional and thermal parameters from the final cycle of refinement (Tables IV–VI), and a stereoview of the molecular geometry of **8** (24 pages). Ordering information is given on any current masthead page.